

Design of Microwave Splitter/Combiner for use in cQED Experiments

472b Senior Thesis
Jared Schwede
Advisor: Rob Schoelkopf

Contents

Acknowledgements	ii
I. Motivation	1
II. Introduction to Couplers	1
a. Branchline Hybrid	2
b. Coupled Line Hybrids	3
i. Lange and Similar Couplers	4
ii. Tandem Couplers	5
III. Experiments and Results	6
a. Validation of Tandem	6
b. Double Bend Tandem Prototype	7
c. Double Bend Tandem	8
IV. Solutions to Measurement Problems	11
V. Concluding Remarks	14
Bibliography	15
Appendix A: Analysis of N-window Branchline	A1
Appendix B: Code	A8

Acknowledgements

I would like to thank Rob Schoelkopf, Blake Johnson, Andrew Houck, Daniel Santavicca, and Luigi Frunzio, who were all pivotally important to this project's success. I would like to thank Dave Schuster for first getting me excited about the work done in the lab and then giving advice as to how to track down and corner Rob. I would also like to thank Professor Barrett for guidance during my time at Yale and for listening to my presentations and for reading this thesis.

I. Motivation

The Schoelkopf Lab is in need of a more sensitive amplifier for its circuit QED (cQED) experiments. The proposed solution to this problem would combine the signal from a cavity with a pump on a line of Josephson junctions. The signal and pump could mix due to the nonlinear inductance of the Josephson junctions, which would potentially allow amplification of the signal. The pump and signal would need to be at similar frequencies, and thus it is pivotal that the pump be isolated from the cavity so as not to unintentionally drive it. The focus of my work in the Schoelkopf Lab has been to develop what is known in microwave engineering as a quadrature hybrid coupler, which is analogous to a power splitter or a half silvered mirror, for this purpose.

I will first state the requirements for our coupler and review typical coupler geometries. I will argue for the geometry I chose, which is known as a tandem coupler, before discussing three sets of experiments. The first experiments validated the tandem geometry. The second set consisted of tests on a larger prototype of an alteration I made to the design, and the third were tests of that design at the target frequency of 6 GHz.

II. Introduction to Hybrids

Working in the microwave range provides interesting opportunities and difficulties because photon wavelengths are on the order of length scales possible to fabricate on a chip. For instance, whereas 60 Hz, the frequency of an ordinary wall outlet, corresponds to a wavelength in air of 5000 km, the wavelength of 60 GHz on silicon is about 16 mm. The fact that phase matters can cause headaches, but it also allows for complicated behavior from deceptively simple designs. This is true in the case of hybrid couplers.

Couplers are symmetric four port devices. An input signal is split between two output ports, commonly called through and coupled ports. Ideally, none of the signal would be reflected, and none would be transmitted to the fourth port, which is called isolated port. The symbol for a hybrid is in Figure 2. Typically, this figure is drawn so that the isolated ports are on the same side – that is, ports 1 and 4 are isolated from each other, as are 2 and 3 – and the through port is directly opposite the input – 2 and 1 are each other’s through ports and similarly for 3 and 4. The final port is the coupled port. 1 and 3 are coupled ports, as are 2 and 4. We desire an even 50/50 split between the through and coupled port. This division is the most common in the literature, although others are possible. An amplitude balance (defined as the difference in dB between the through and the coupled ports) of less than 1 dB is frequently desired. We also would like a 90° phase difference between these two ports. Complete absence of reflection and total isolation are not generally attainable, and a more realistic goal is to keep these ports below -15 or -20 dB, which correspond to about 3% and 1% power transmissions respectively. These requirements on the ports should be maintained for as large of a bandwidth as possible.

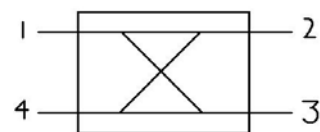


Figure 1: Hybrid Coupler

The Schoelkopf Lab has cQED experiments between 5 and 7 GHz, and so any coupler design would need to work over this range of frequencies. This means that, at a minimum, a coupler centered at 6 GHz would need a fractional bandwidth of 33%. However, so that this coupler could be used in future experiments at slightly different frequencies, a larger bandwidth should be aimed for, preferably an octave. We would like to integrate two of these couplers with Josephson junction lines between them on a 2x7 mm chip, which puts a serious constraint on the size, since a quarter wavelength, which most 90° hybrid geometries require, at 6 GHz on silicon is about 4 mm. To eliminate resistive loss, we will use niobium. When used in cQED experiments, this chip will likely be integrated around 10 mK, but because of niobium's high critical temperature, about 8 K, for tests, a simple helium dunker will suffice. Chips are made on both silicon and sapphire, so a design that would function on either would be valuable.

Microwave engineering of this sort is most commonly done in either microstrip or coplanar waveguide (CPW) (Figures 3 and 4). In microstrip, a thin strip of metal is separated from a ground plane by a dielectric layer. Coplanar waveguide has ground planes on both sides of a middle strip and can also have a backing ground plane like in microstrip. The Schoelkopf lab uses CPW almost exclusively, as having an easily accessible ground plane provides advantages, although ensuring that these ground planes are well connected can cause trouble.

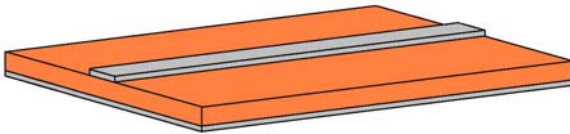


Figure 5: Microstrip

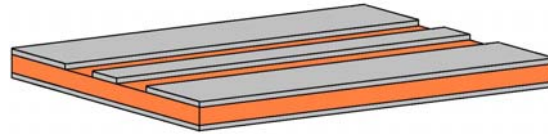


Figure 6: Coplanar Waveguide

While there are other variations, Quadrature hybrids in microstrip or coplanar waveguide can be broadly categorized into three main types: branchlines, lumped element, and coupled lines. Although successful lumped element designs do exist, some of which can extend a design's bandwidth while decreasing overall size,¹ these tend to be more complex to design than other couplers, and I did not feel that these were realizable given our requirements, especially our requirement of low temperature. I will discuss branchline couplers before examining coupled line hybrids, which fit the constraints of this problem better.

II. a. Branchline Hybrids

In general, a branchline hybrid can have any number of "windows." The simplest, an example of which can be seen in Figure 4,ⁱⁱ has just one.¹ Branchlines are perhaps

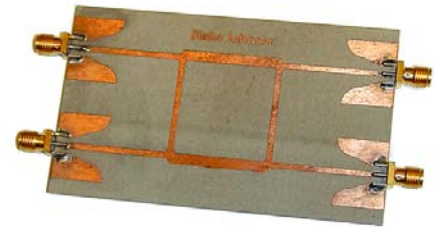


Figure 4: Single Window Branchline

¹ Although it is not consistent with much of the literature on them, I will refer to branchlines as having a number of windows instead of a number of branches. The number of windows is much clearer to me, and it has the additional advantage that counting the complexity (the number of windows or number of branches)

the most theoretically straightforward hybrids. If one requires that at a center frequency, exactly half the power goes to each coupled port, then one can derive analytic expressions for the line impedances using even-odd mode analysis.² From these analyses, one can gather that bandwidth can be improved with additional windows. However, once there are around three or four windows, the line impedances required to increase bandwidth become difficult to achieve. Thus, three window hybrid is typically the highest used. Examples of these and novel variations of branchline designs can be found in ^{iii iv v}.

Branchlines suffer from two problems that make them an unfortunate choice for our set of constraints. The first of which has already been hinted at. Branchlines' bandwidths are typically very narrow. For the one window branchline, one cannot realistically expect a fractional bandwidth of over around 15%.^{vi} For the three window design, this can be pushed to around 55 to 60%.^{vii} This would certainly be enough to function at both 5 and 7 GHz, but even this is less than many coupled line designs, which frequently have bandwidths of an octave or more.

More importantly, this additional bandwidth comes at the cost of size. Each branch is a quarter wavelength long. Even with space saving modifications as in ^{viii ix}, one could only hope to put a one- or two-window design on a 2x7 chip. Since the goal is to combine two hybrids with two Josephson junction lines in this space, only a one-window design would have hope of working, and its bandwidth would likely be too narrow.³

II. b. Coupled Line Hybrids

If two transmission lines are put close enough to each other, a signal from one line can be transmitted through electromagnetic fields to the other, as illustrated in Figure 6. As can be seen in Figure 5,^x these lines are maximally coupled when their length is a quarter wavelength. Following even-odd mode analysis like that in Pozar, chapter 7, it can be shown that it is difficult to achieve 3 dB coupling using these lines. The major coupled line hybrids find ways around this poor coupling, usually in one of two following ways.

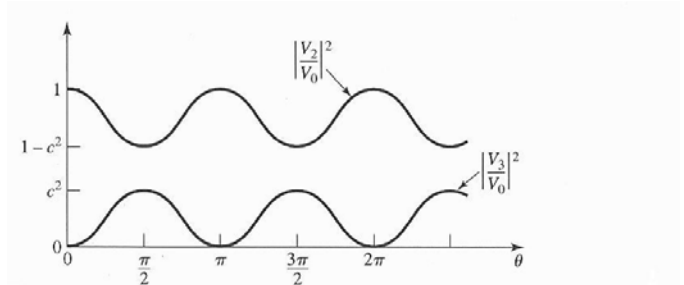


Figure 5: Coupling as a Function of Line Length

starts at one instead of two. To translate, just add one to the number of windows to get the number of branches.

² For more on even-odd mode analysis of hybrids, see Pozar's Microwave Engineering, Chapter 7. For a derivation of the impedance relationships for an N-window branchline, information I have not found elsewhere, see Appendix A.

³ The chip space might be less constrained in the future. If it is increased sufficiently, I might recommend using a branchline design largely due to its simplicity, specifically in its lack of complicated wire bonding. At least one geometry for a single window branchline is as about the size of the design I picked.^{viii}

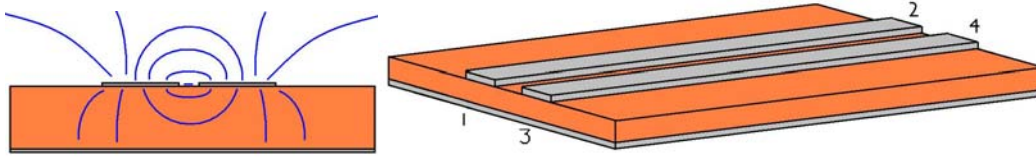


Figure 6: Coupled Lines

II. b. i. Lange and Similar Couplers

The first way to improve coupling is to increase the number of lines that talk to each other. While three line designs are able to achieve 3 dB coupling over a bandwidth of an octave,^{xi xii} they are not as widely used as other designs largely because this coupler is more asymmetric than couplers with even numbers of lines. Four line designs are much more popular, although each additional line increases the complexity. Note that, without modifications, the through and coupled ports (2 and 3 if 1 is the input) are on opposite ends. It is generally desirable to have these two ports adjacent to each other, and so many couplers incorporate a crossover into the design. The famous Lange coupler^{xiii} is a four (or sometimes six) line design with crossover in the middle of the quarter wavelength lines, as can be seen comparing Figures 7 and 8. Without the crossover, a four line coupler is called an “Unfolded Lange.”^{xiv} According to the literature and my Sonnet simulations, bandwidths of about an octave are easily attainable. The design’s use is so widespread that Microwave Office includes a microstrip Lange geometry. However, while Lange couplers are well studied in microstrip, they are far less commonly used in coplanar waveguide. Although CPW treatments can be found,^{xv} the design of these couplers is far more difficult in the coplanar geometry than in microstrip. Not only does Microwave Office have no CPW Lange design, but it has no model for four coupled lines in CPW – only two and three. This means that all simulations would have to be done in Sonnet, which, while likely accurate, would be exceedingly time consuming. Since the setup of the chip and board lends itself much easier to CPW geometriesthis is a large blow for any design with four or more lines.

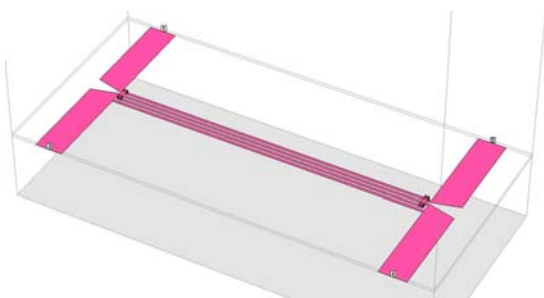


Figure 7: Unfolded Lange

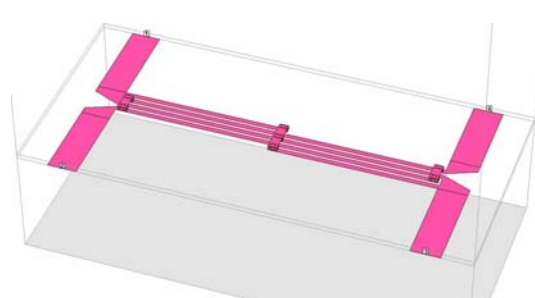


Figure 8: Lange Coupler

II. b. i. Tandem Couplers

Another solution to the coupling problem is to use what is called a tandem coupler, which can be understood as putting two poor couplers in series, as in Figure 9. This design is not as popular in microstrip, largely because of difficulties isolating the two couplers from each other. In CPW, there is a ground plane between these couplers, which makes separating them much simpler. Chang, Liao, and Chen reported a CPW tandem in 2003 with a 2 dB amplitude balance bandwidth of 91%, with return loss and isolation better than -18 dB in this frequency range.^{xvi}

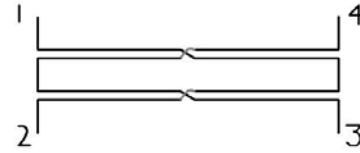


Figure 9: Tandem Coupler

This amplitude imbalance is larger than would probably be desired, but these results compare favorably with the Lange coupler. Both the Lange and the tandem have four parallel lines in total, and both are a quarter wavelength long and are quite narrow. Since the tandem separates its lines by a ground plane, a tandem will likely be 50-100% wider than a comparable Lange. Instead of the design process being hampered by the choice of CPW, the tandem is enhanced, and it can fully use CPW's advantages over microstrip. In addition to consistency with previous Schoelkopf Lab experiments, using CPW allows additional flexibility in choosing the line widths and sizes of gaps. These can be shrunk to essentially as small as is possible to fabricate. As stated above, simulation is significantly easier for the tandem, and simulation results can be cross validated between Microwave Office and Sonnet.

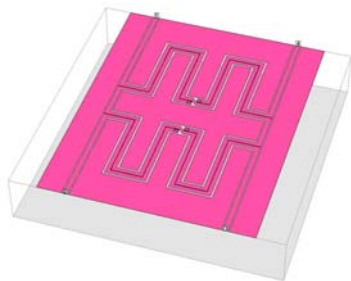


Figure 10: Double Bend Tandem

With just these comparisons, I feel the tandem is the most natural choice. However, the largest advantage of the tandem is that its two line design allows for meandering would not be possible for a design with more lines. An example of such a double bend design can be seen in Figure 10. With these bends, it is possible to turn a design that is narrow and long into one with much more balanced dimensions. According to simulations, this does not adversely seriously affect

performance. To my knowledge, my alterations make this the only coupler design with such a large bandwidth whose largest dimension is as small as an eighth wavelength. Two of these lines can fit snugly onto a 2x7 mm chip with Josephson junction lines up to 3-4 mm long between them, as in Figure 11.

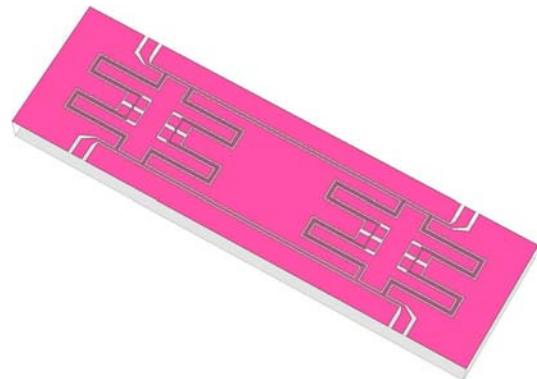


Figure 11: Full Chip Setup

III. Experiments and Results

In all that follows, unless otherwise noted I will use S21 to mean the through port, S31 to mean the coupled port, S41 to be the isolated port, and S11 to be the reflection. This implicitly assumes that the responses from each port are identical, an assumption that is very nearly valid (deviations from it will be discussed in the prototype section).

III. a. Validation of Tandem

Before testing my bendy alteration, I made a test of the original tandem design. Prototypes were made with copper on 62 mil FR-4 (dielectric constant: 4.35 at 500 MHz, loss tangent: 0.01), and they were centered at around 450 MHz. The quarter-wave lines were about 3.6 inches long. The spacing between the lines was 5 mils, which was the



Figure 12: Tandem Prototype

smallest available spacing from Sierra Protoexpress (protoexpress.com), the company used to make the boards, and the line width was 50 mils. I tested three different sizes of gap between line and ground plane: 5, 10, and 20 mils. In addition, I had these designs made either with or without vias connecting the ground planes to the back of the board. I used vias in Sonnet, largely for speed and ease of simulation. The results for the 20 mil gap test can be seen in Figures 15 and 16 and compare favorably with simulation, Figure 14. Overall, the results are very similar to Chang, Liao, and Chen's. The design without vias has an unwanted spike around 650 MHz. This was due to the outer ground planes (the uppermost and lowermost ground planes in Figure 12) not being sufficiently grounded. Shorting these ground planes to the backside eliminates this problem. It is

expected that this will not be an issue for the double bend tandem on the chip for two reasons. First, the analogous ground planes in the double bend are about half the length of these, and thus any resonances would be at about twice the frequency. Second, the 2x7 mm chips are well grounded everywhere along the edge of the chip. For this and the double bend designs, only ~5 wire bonds were sufficient where wire bonding was required. There were several possible wirebond patterns. The one with the fewest required bonds is shown in Figure 13.

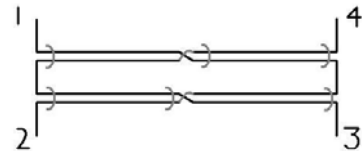


Figure 13: Wirebond Pattern

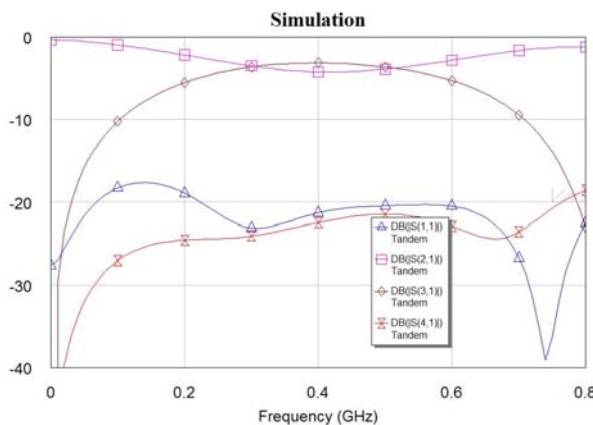


Figure 14: 20 mil gap simulation

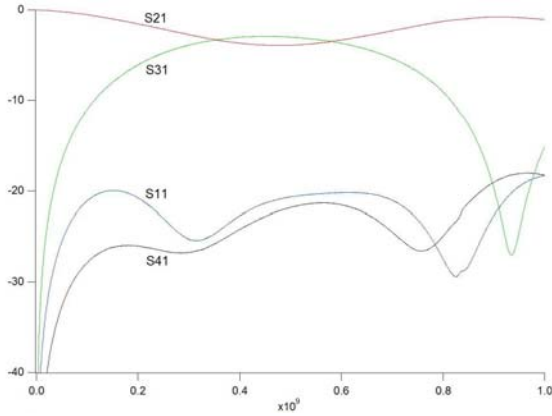


Figure 15: 20 mil gap with vias

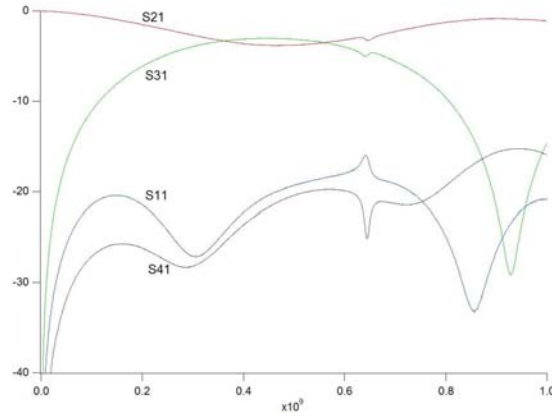


Figure 16: 20 mil gap without vias

III. b. Double Bend Tandem Prototype

Double-bend tandems were then made, again on 62 mil FR-4. The width of line and spacing between them were 50 and 5 mils, as before. The gap to the ground plane was 20 mils. I also had designs with 30 mil gaps, but the 20 mil gaps performed satisfactorily and I saw no need to test the 30 mil designs.



Figure 17: Double Bend

I had three sets of double bend designs that varied, essentially, how squashed they were. As can be seen in Figures 19 and 20, the results of the least and most bendy were very similar. I once again had boards with and without vias made, and the minimal successful wire bonding pattern is summarized in Figure 18. The boards without vias performed very well, and, as expected, resonances are pushed higher and out of the desired range (Figure 21). Overall, the results were very good, with bandwidth of nearly an octave (~270 to 530 MHz) with amplitude balance of < 1 dB, reflection and isolation < -20 dB, and a phase differences of $90.5 \pm 0.5^\circ$.

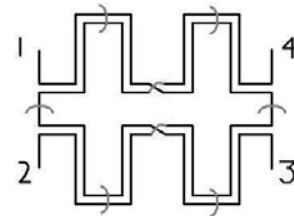


Figure 18: Bonding Pattern

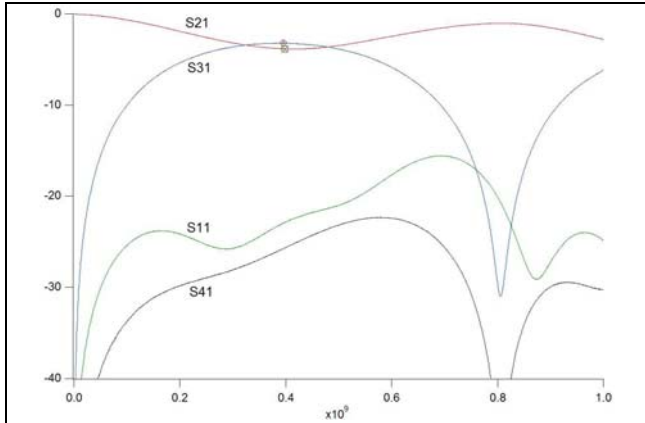


Figure 19: Extra Bendy with vias

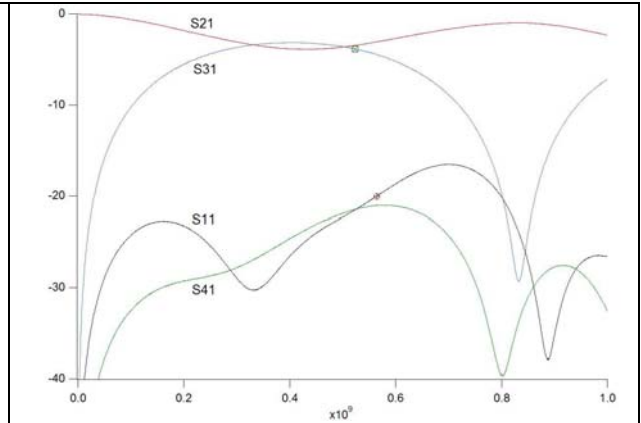


Figure 20: Not so Bendy with vias

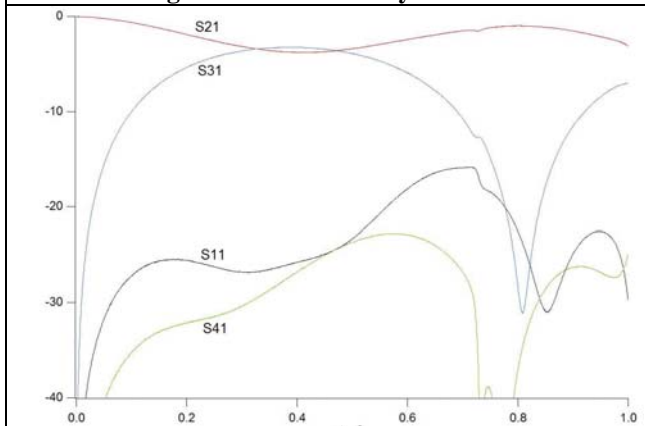


Figure 21: Extra Bendy without vias

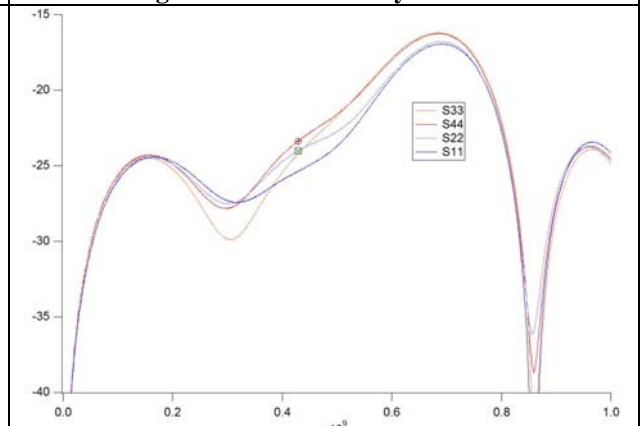


Figure 22: Extra Bendy with vias Reflection

Figure 22 demonstrates that reflections from the different ports in the most bendy design with vias were not identical. I believe that these deviations were due to the crossover. If at the first crossover it meets, the line is connected by wire bonds (i.e. if it is the line that is crossing over), then there is a “hump” around 400 MHz. This is true for S44 and S22. If at the first crossover, the line crosses under, as is the case for S11 and S33, there is no such hump. Additionally, two of the reflection measures, S33 and S44, are overall higher than the other two, S11 and S22. Note ports 3 and 4 are mutually through, as are 1 and 2. This difference can be explained by noting that the crossover connecting port 3 and 4 had fewer and longer wire bonds. Essentially, it was a poorer crossover. Since only one wire bond will be possible per crossover in the test design, even with the shortening of the required length of this bond, these differences and problems may be exacerbated.

III. c. Double Bend Tandem

The 2x7 mm chips used in the Schoelkopf Lab are planted into recesses in circular boards of AR1000 (dielectric constant: 10 at 10 GHz, loss tangent: 0.001) with diameter of 3 cm. There are eight entry points to the chip, three from each side and one on each end. My test of the tandem designs used four of them (Figure 23). The

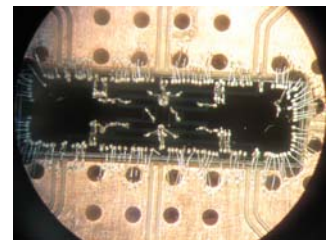


Figure 23: Tandem on Chip

ground planes on the board were bonded to the chip, and lines on the board were connected to corresponding launchers on the chip by at least three wire bonds. My launchers were slightly different from earlier launchers, and so in addition to tandem designs, the launchers on one chip were simply connected with an approximately 50Ω line of width $30 \mu\text{m}$ and gap size $20 \mu\text{m}$. Three variations of the same tandem were created in niobium on silicon (dielectric constant: 11.9 at 10 GHz, loss tangent: 0.01), although the tandems were designed to function on sapphire as well.⁴ These differed in the width of line and the space between the lines and the ground planes, as summarized by Table 1.⁵

Table 1: Tandem Dimensions

Name	Spacing	Line width	GP Gap
w25	$10 \mu\text{m}$	$25 \mu\text{m}$	$15 \mu\text{m}$
w35	$10 \mu\text{m}$	$35 \mu\text{m}$	$15 \mu\text{m}$
w20	$10 \mu\text{m}$	$20 \mu\text{m}$	$20 \mu\text{m}$

The wafer was originally to be $500 \mu\text{m}$ silicon. However, the only wafers available were $300 \mu\text{m}$. According to both Sonnet and Microwave Office simulations, this did not adversely affect the design's performance, since the distance to ground planes on the chip was either 15 or $20 \mu\text{m}$. I stacked two of these $300 \mu\text{m}$ chips in the board recess. Doing so meant that boards without a backing ground plane in the recess had to be used, and there were only two of these types of boards.

This wafer also served as a test of in-house mask creation. Table 2 summarizes the fabrication results. Overall, about 80% of the designs were useable. Two types of the design, the $35 \mu\text{m}$ width and the $20 \mu\text{m}$ width, had systematic errors – protrusions in a line connected to the launcher, as can be seen in Figures 24 and 25. According to a Sonnet simulation, however, these protrusions would have little effect on the results.

Table 2: Fabrication Results

	Useable	Unuseable	%
w25	12	6	67%
w35	14	4	78%
w20	14	4	78%
Launcher	17	1	94%

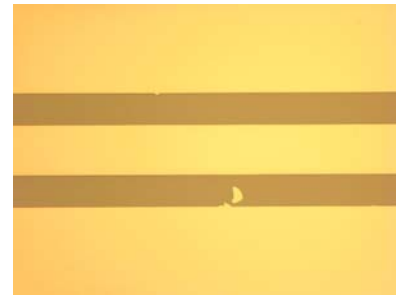


Figure 24: w20 Protrusion

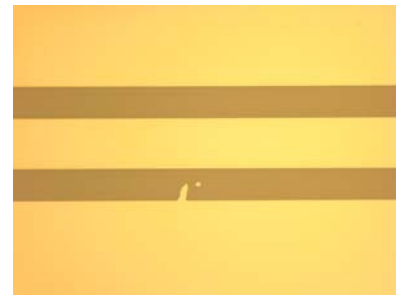


Figure 25: w35 Protrusion

⁴ While the designs would work on sapphire, the mask would need to be remade. The spacing between the chips was only $200 \mu\text{m}$, which is slightly too small for the most narrow blade usable for dicing sapphire.

⁵ This sort of alteration is very easy to do because of Sonnet's parameters feature. A file that includes all relevant parameters is in U:/Jared/chip simulations/FOR CHIP s 10.son. These can then be exported in dxf format and opened in AutoCAD

The board and chip were put in a copper casing and into a helium dunker (Figure 26). The shift from the prototype to superconducting versions created two main difficulties. Firstly, wire bonding became much more difficult. I added 150 μm pads at the crossover in order to make wire bonding possible (Figure 27), but even with these comparatively large pads, wire bonding was still very difficult. I only succeeded in completely wire bonding about 30-50% of the chips I attempted.

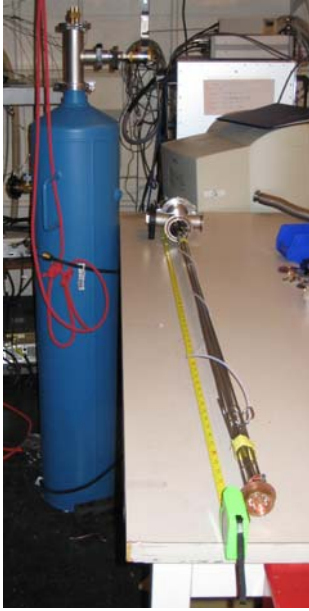


Figure 26: Dunker and Cables

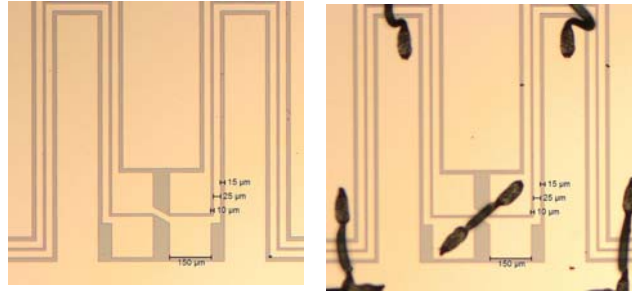


Figure 27: Crossover Pads

Because of time constraints and the limited number of chips, I was not able to fully test for differences in wire bond patterns on the chip. The wire bonding that I performed can be summarized by Figure 28. Essentially, I tried to connect the floating center ground plane in as many places as possible while minimizing the number of difficult wire bonds.⁶

The wire bonding for the test of the launcher can be deduced from the simulation image (Figure 29).

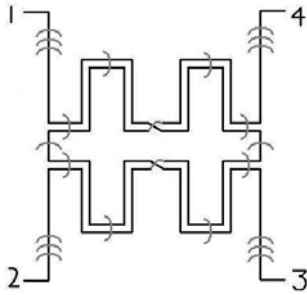


Figure 28: Tandem Bonding Pattern

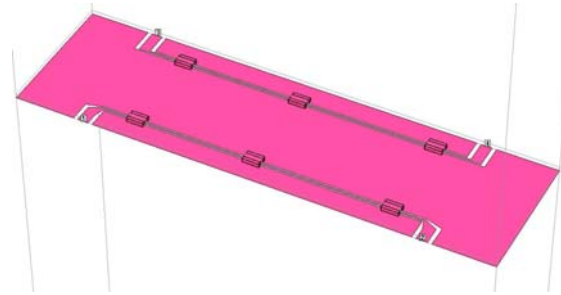


Figure 29: Launcher Bonding Pattern

The second problem was calibration. The chip was connected through dunker cables that were more than a meter long. Unlike in the case of the prototypes, where all cables connected to the board were part of the calibration, there was no obvious way to calibrate these cables away. These stainless steel cables were very lossy and had finite reflection at each end on the order of -20 dB. This meant that reflections of the through and coupled lines would be on the order of the S11 and S41 signals we wanted to measure. Reflections like these led to wild fluctuations in the isolated and reflected port signal, as in Figure 30, which shows the 25 μm width results from an input port 2. In addition, the

⁶ Wire bonding could be entirely avoided by having a multilayer substrate with vias, although, at this point, this may be beyond our capabilities

length of the cables essentially scrambled the phase information, and I have not been able to think of a way to recover it.

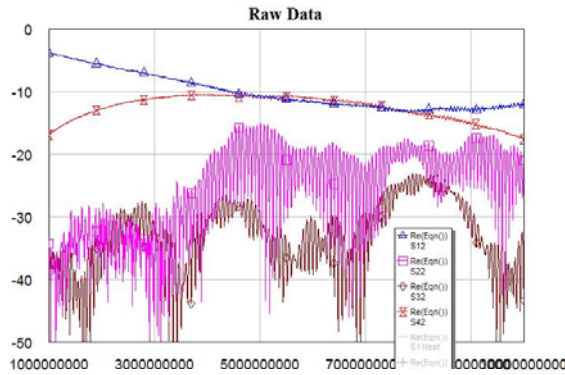


Figure 30: Chip Tandem

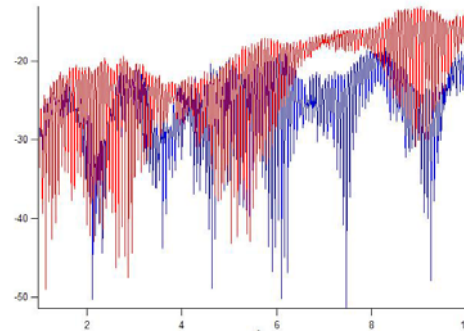


Figure 31: S11 vs. S22

IV. Solutions to Measurement Problems

The first potential solution would be to add back the attenuation to the port parameters. This has advantages in simplicity, and the launchers test could be used a measure of cable attenuation, since Sonnet simulations suggest its transmission is better than -0.05 dB. This would likely work well for S21 and S31, but because the effects seen in S11 and S41 may be a complicated mix of all four of the hybrid’s outputs, it is less likely to be successful for these ports. Additionally, unless additional fitting is involved, this does not get rid of resonances. It also makes assumptions about constancy between cables and between ports, whereas it does appear that different cables may have different behaviors, as can be seen in a comparison of w35’s measured S11 and S33 (Figure 31), which, considering the discussion in the prototype section about crossovers, should be most similar. Additionally, these reflection measures show cross experiment similarity – that is, w25’s S11 measure is very similar to w35’s S11 measure.

Another, related solution would be invent port parameters for the coupler and then run these through a reasonable simulation of the long cables. Although the attenuation and the reflection of the cables are not difficult to ascertain, a realistic model for the cables’ interfaces is not necessarily simple to create. This could lead somewhat arbitrary data generation which would be fitting an incorrect model instead of representing actual parameters of the tandem. Because this method required no hardware alterations and allowed me to analyze the data we already gathered, this is what I focused on. So that data generation would be simple and would not become arbitrary, I kept the data creation

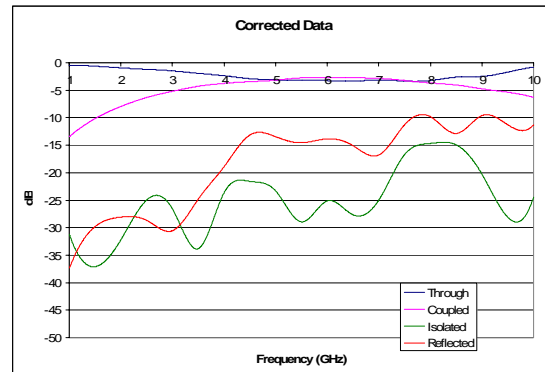


Figure 32: Corrected Results

grounded in measurements. I used the results from the 25 μm line width, 15 μm gap size. First, to remove the wild resonances, I fit the measured S-parameters using cubic splines with 20 knots.⁷ There was some overfitting, especially in S11, but the overall results were acceptable. I also fit the launcher test in a similar fashion. I then subtracted the launcher test from these fitted S-parameters. As stated above, this is likely very nearly valid for the through and coupled ports but not as likely to be realistic for the other two ports. Unfortunately, as mentioned previously, no phase information was available. I thus used phase data from a Sonnet simulation. The result of this process is shown in Figure 32.⁸

I then created a model of the lines in MWO. The only information we could gather was an approximate magnitude of the reflection from the cables. Since the reflection had similar magnitudes on each end, this setup can be suitably modeled by having long cables with impedance that differs from 50 Ω . An impedance of 55 Ω yields a suitable reflection coefficient.⁹ The results of this simulation are in Figure 33. This simulation makes several assumptions, not all of which do I believe to be valid. For one, it assumes that the reflection coefficient (both its phase and magnitude) are independent of frequency, which, given the magnitude of the reflection trace below 3 GHz, is almost certainly false. As stated before, the phase information for the four ports and that for the cable interface was invented, and it is clear from the isolation trace that this simulation does not capture all of the behavior. For these reasons, I believe that improving the performance of this model would more likely be fitting an incorrect simulation instead of making the tandem's S-parameters more realistic.

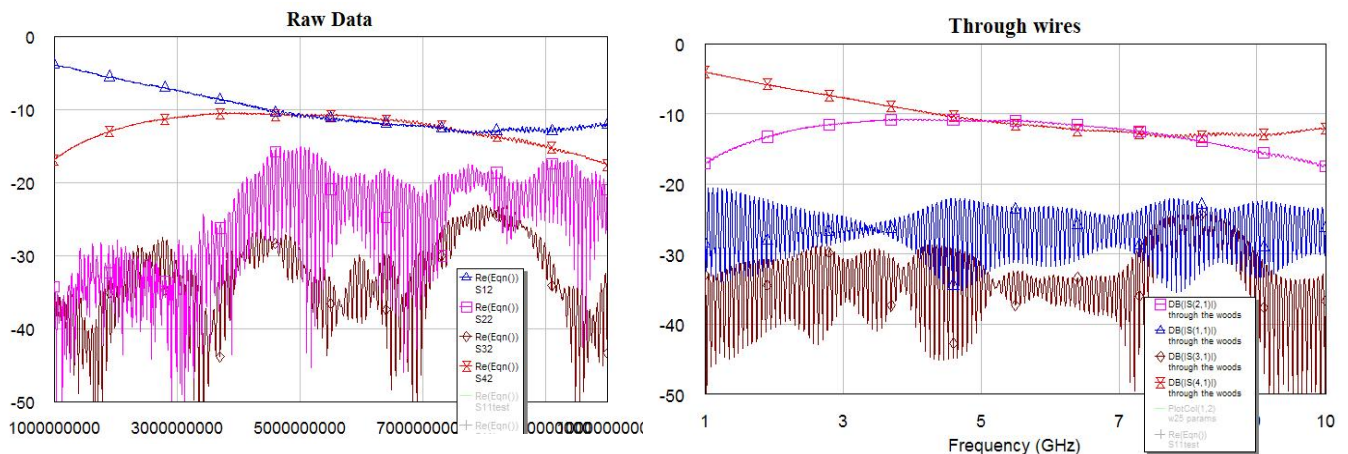


Figure 33: Corrected results through MWO Lines

Nonetheless, it is possible to gain some information from this model. We have already noted that this model is likely realistic when analyzing the through and coupled lines. The amplitude balance between these ports is less than 1 dB from around 4.22 to 8.28 GHz, a

⁷ R code in Appendix B

⁸ I used an Excel macro to put the data into a form MWO liked. This code is also in Appendix B.

⁹ Note that that an impedance of 46 Ω yields a similar reflection coefficient. Since we lack phase information about the line interface, it is unclear which of these should be used. This choice's effect on the outcome is not negligible and reinforces the idea that the creating a better fit to the model is not necessarily the same as creating realistic port parameters.

fractional bandwidth of 65%, which is just shy of an octave and very similar to the prototype results.

It also appears that our guess for the isolation is probably relatively accurate, even if some of its structure was likely invented by the splines used to fit. If this is true, then we can say that the isolation is better than -20 dB below around 7-7.5 GHz and is likely always better than around -14 or -15 dB. Neglecting reflection for a moment, these are properties of a very good coupler.

We cannot gather much about the tandem's reflection from our measured parameters. We can, however, put an upper limit on it and the isolated port by examining the remainder of the signal after subtracting the through and coupled ports. However, we must keep in mind that our assumption that our launchers had unity transmission is not entirely accurate and that our spline fit may have been slightly off. We can correct for this by allowing our launchers to be α dB from perfect transmission. In Figures 34 and 35, the green lines are the maximum allowed values for reflection and isolation for $\alpha = 0.5$ and $\alpha = 1$. Since Sonnet simulations put the maximum deviation from unity transmission at better than -0.05 dB, and since the amplitudes of the wiggles in the through and coupled lines are never larger than about 0.8 dB, I believe we can reasonably expect the maximum value of α to be between these two values. If this assumption is correct, then the reflection is likely less than around -15 dB until at least 7-7.5 GHz. Together with the results of this analysis for the other ports, this makes for a very respectable coupler.

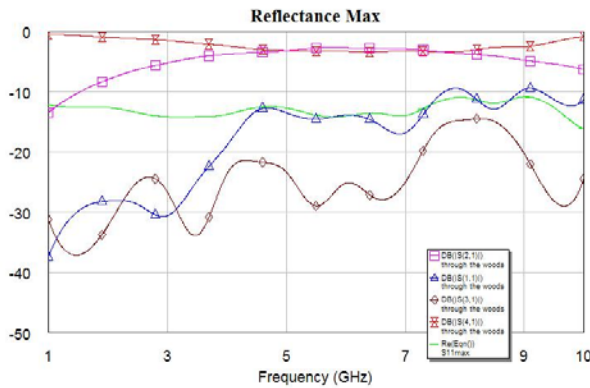


Figure 34: Max S11 and S41, $\alpha = 1.0$

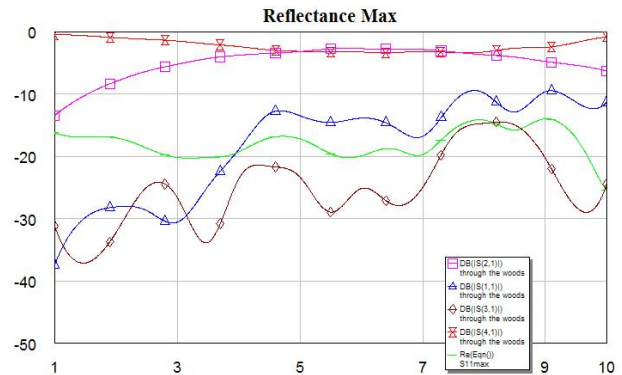


Figure 35: Max S11 and S41, $\alpha = 0.5$

Since the above analysis cannot, in my opinion, be taken any further, I believe a modification to the hardware is required to gain additional information. One straightforward alteration would be to make a shorted or open board, that is, to have no chip in the recess and to either leave the lines on the board unconnected, forming an open, or short them to a neighboring ground plane. In analogy to treating the launcher test as a through, having this open/short data might help in doing after the fact calibration. I am unsure, however, that this would be all that informative. One would hope to gain information about the reflection this way, but it's very possible that the reflection depends in a complicated manner on the hybrid and the other ports. Nonetheless, since this modification is simple and nonpermanent, I believe it would be valuable.

Since much of the contribution to the isolated port's resonances is due to reflection of the through and coupled ports, it may make sense to try to terminate these on the board. Using the data generated above, according to a Microwave Office simulation (Figure 36), these terminations may eliminate almost all of the wiggles and may allow us to faithfully recreate this port's response. This analysis again makes assumptions about constancy between experiment and between ports. The simulation suggests that this modification would have little effect on the reflection. I believe this is because the coupled and through ports, after passing through the tandem twice, are very close to 180° out of phase. It should also be noted that the terminations may have nonzero reflection coefficients. This modification would be rather permanent, and there are only two boards without copper backing, meaning a mistake might preclude the possibility of any other tests. Nonetheless, because of the potential information to be gained about the isolated port, I believe this to be an excellent next step.

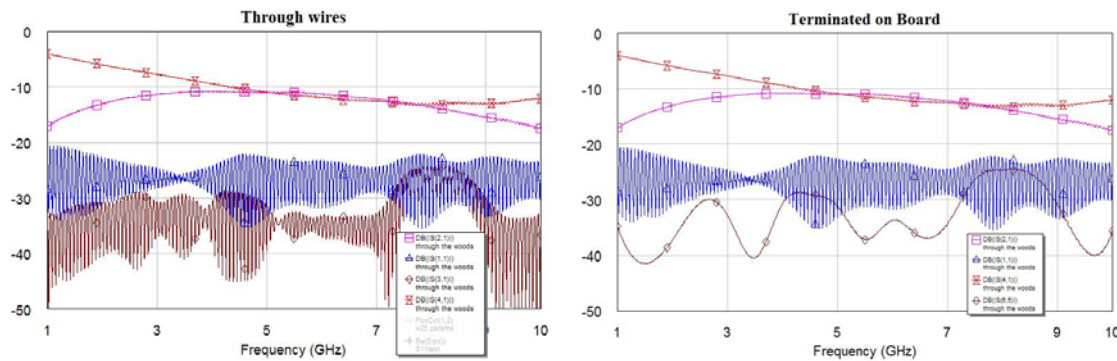


Figure 36: S21 and S31 Terminated

V. Concluding Remarks

Despite the problems I have had analyzing the superconducting tandems, I am, overall, satisfied with the results. In summary, what we do know about the tandem design seems promising. I believe that the isolation is almost certainly below -20 dB at 5 and 7 GHz. I am not aware of a method to determine more about the reflection or the phase, although altering the design of the cables to allow for easier calibration may make such measurements possible and would likely be a valuable change for other experiments in the lab. Until then, the modifications above, specifically terminating the through and coupled ports on the board, should be pursued. I believe that deviations from simulation, including the higher S41 and S11 parameters, may be due to the small number of wire bonds possible to put on the chip. The crossover pads should be enlarged in order to make wire bonding easier and so that perhaps more than one bond could be used, and the design of the crossover should be reevaluated. I think that using multilayer substrates, which would eliminate the need for difficult wire bonding, should be investigated. If or when the chip's size is changed, other geometries, specifically branchline structures, may be easier to fabricate. I think these tandems should be combined with Josephson junction lines as soon as possible and that tests should begin on these.

Bibliography

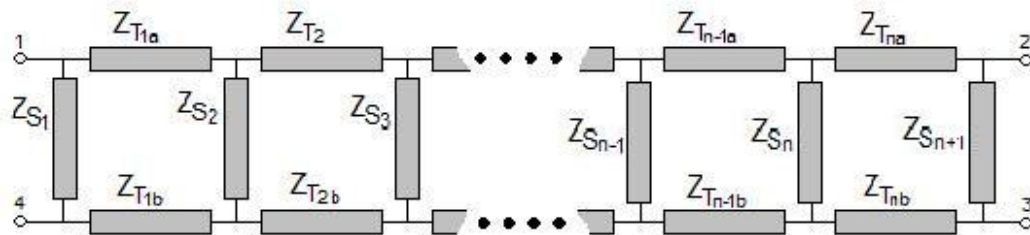
- ⁱ D. P. Andrews and C. S. Aitchison, “Wide-band lumped-element quadrature 3-dB couplers in microstrip,” *IEEE Trans. Microw. Theory Tech.*, vol. 48, no. 12, pp. 2424–2431, Dec. 2000.
- ⁱⁱ Blake Johnson, presentation for Prof. Schoelopf’s Microwave Engineering Course, Spring 2006.
- ⁱⁱⁱ M. Muracuchi, T. Yukitake, and Y. Naito, “Optimum design of 3-dB branch-line couplers using microstrip lines,” *IEEE Trans. Microw. Theory Tech.*, vol. MTT-31, no. 8, pp. 674–678, Aug. 1983.
- ^{iv} B. Mayer, “New Broadband Branchline Coupler,” *Electron. Lett.*, vol. 26, pp. 1477–1478, Aug. 1990.
- ^v D. K. Paul, P. Gardner, B. Y. Prasetyo, “Broadband Branchline Coupler for S Band,” *Electron. Lett.*, vol. 27, pp. 1318–1319, Jul. 1991.
- ^{vi} www.microwaves101.com/encyclopedia/Branchline_Couplers.cfm
- ^{vii} Y. H. Chun, J. S. Hong, “Compact Wide-Band Branch-Line Hybrids,” *IEEE Trans. Microwave Theory Tech.*, vol. 54, pp. 704–709, Jun. 2006.
- ^{viii} H. Ghali and T. A. Moselhy, “Miniaturized fractal rat-race, branch-line, and coupled-line hybrids,” *IEEE Trans. Microw. Theory Tech.*, vol. 52, no. 11, pp. 2513–2520, Nov. 2004.
- ^{ix} S. S. Liao, P. T. Sun, N. C. Chin, and J. T. Peng, “A novel compact-size branch-line coupler,” *IEEE Microw. Wireless Compon. Lett.*, vol. 15, no. 9, pp. 588–590, Sep. 2005.
- ^x D. M. Pozar, *Microwave Engineering*, 3rd ed. New York: Wiley, 2005.
- ^{xi} V. Tulaja, B. Schiek, J. Köhler, “An Interdigitated 3-dB Coupler with Three Strips.” *IEEE Trans. Microw. Theory Tech.*, vol. 26, no. 9, pp. 643–645. Sep. 1978.
- ^{xii} J. C. Chiu, J. M. Lin, M. P. Huong, Y. H. Wang, “A PCB-Compatible 3-dB Coupler Using Microstrip-to-CPW Via-Hole Transitions,” *IEEE Microw. Wireless Compon. Lett.*, vol. 16, no. 6, pp. 369–371, Jun. 2006.
- ^{xiii} J. Lange, “Interdigitated stripline quadrature hybrid,” *IEEE Trans. Microwave Theory Tech.*, vol. MTT-17, pp. 1150–1151, Dec. 1969.
- ^{xiv} R. Waugh and D. LaCombe, “Unfolding the Lange coupler,” *IEEE Trans. Microw. Theory Tech.*, vol. MTT-20, no. 11, pp. 777–779, Nov. 1972.
- ^{xv} P. Pieters, S. Brebels, E. Beyne, R. P. Mertens, “Generalized Analysis of Coupled Lines in Multilayer Microwave MCD-D Technology – Application: Integrated Coplanar Lange Couplers,” *IEEE Trans. Microw. Theory Tech.*, vol. 47, no. 9, pp. 1863–1872 Part 2, Sep. 1999.
- ^{xvi} T. Y. Chang, C. L. Liao, C. H. Chen, “Coplanar-waveguide tandem couplers with backside conductor,” *IEEE Microwave and Wireless Components Letters*, vol. 13, pp. 214–216, Jun. 2003.

Appendix A

Analysis of Branch-Line Hybrids

Following the notation and method of Pozar, 3rd Ed, Ch 7

Derivation of Useful Relations



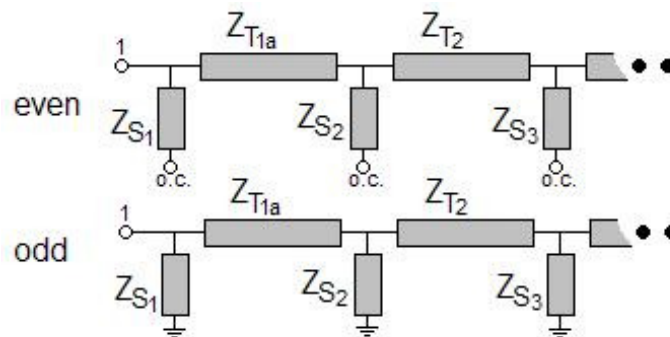
Consider the n-window branchline hybrid, with all lengths $\lambda/4$. We can use even/odd mode analysis to split this four-port network into two two port networks and thus try to determine the impedences of the transmission lines (normalized so that the port impedance is 1) such that the amplitudes of the emerging waves are subject to the following constraints:

$$B_1 = \frac{1}{2} \Gamma_e + \frac{1}{2} \Gamma_o = 0$$

$$|B_2| = \left| \frac{1}{2} T_e + \frac{1}{2} T_o \right| = \frac{1}{\sqrt{2}}$$

$$|B_3| = \left| \frac{1}{2} T_e - \frac{1}{2} T_o \right| = \frac{1}{\sqrt{2}}$$

$$B_4 = \frac{1}{2} \Gamma_e - \frac{1}{2} \Gamma_o = 0$$



Where B_i is the amplitude of the emerging wave from port i , Γ and T are the reflection and transmission coefficients respectively, and the incoming wave has total amplitude 1. Adding and subtracting equations 1 and 4, and noting power conservation, we write these more simply as:

$$\begin{aligned} \Gamma_e = \Gamma_o = 0 \\ |T_e + T_o| = |T_e - T_o| \end{aligned}$$

We have implicitly declared port 1 to be the incoming port, but we would like any port to be able to serve equally well as an incoming port. Requiring this imposes a symmetry on the transmission lines so that the n -window hybrid has $n+1$ unique impedances, $Z_{S_{n+1}} = Z_{S_1}$, etc. The shunt impedances are found using (2.44) in Pozar:

$$\begin{aligned} Z_{L,e} = \infty, \quad Z_{L,o} = 0, \quad l_s = \frac{\lambda}{8}, \\ Z_{S,e} = Z_S \frac{Z_{L,e} + iZ_S \tan[\beta l_s]}{Z_S + iZ_{L,e} \tan[\beta l_s]} = -iZ_S \\ Z_{S,o} = Z_S \frac{Z_{L,o} + iZ_S \tan[\beta l_s]}{Z_S + iZ_{L,o} \tan[\beta l_s]} = iZ_S \end{aligned}$$

And the ABCD matrices for the shunts and transmission lines are found using Table 4.1:

$$\begin{aligned} \mathbf{ABCD}_{S,e} = \begin{pmatrix} 1 & 0 \\ \frac{i}{Z_S} & 1 \end{pmatrix}, \quad \mathbf{ABCD}_{S,o} = \begin{pmatrix} 1 & 0 \\ -\frac{i}{Z_S} & 1 \end{pmatrix} \\ \mathbf{ABCD}_{T,e} = \mathbf{ABCD}_{T,o} = \begin{pmatrix} \cos[\beta l_T] & iZ_T \sin[\beta l_T] \\ \frac{i \sin[\beta l_T]}{Z_T} & \cos[\beta l_T] \end{pmatrix} = \begin{pmatrix} 0 & iZ_T \\ \frac{i}{Z_T} & 0 \end{pmatrix} \end{aligned}$$

Noting that

$$\begin{aligned} \mathbf{ABCD}_{S,o} = \mathbf{ABCD}_{S,e}^* \\ \mathbf{ABCD}_{T,o} = -\mathbf{ABCD}_{T,e}^* \end{aligned}$$

and since the even ABCD matrix for the whole n -window branchline hybrid is given by:

$$\mathbf{ABCD}_e = \mathbf{ABCD}_{S_1,e} \mathbf{ABCD}_{T_1,e} \mathbf{ABCD}_{S_2,e} \mathbf{ABCD}_{T_2,e} \dots \mathbf{ABCD}_{T_n,e} \mathbf{ABCD}_{S_n,e} \mathbf{ABCD}_{T_1,e} \mathbf{ABCD}_{S_1,e}$$

(and likewise for odd), we see that

$$\mathbf{ABCD}_o = \pm \mathbf{ABCD}_e^*$$

with + for n even and - for n odd. For $n=1$, the even matrix is:

$$\mathbf{ABCD}_{e, n=1} = \begin{pmatrix} 1 & 0 \\ \frac{i}{Z_S} & 1 \end{pmatrix} \cdot \begin{pmatrix} 0 & iZ_T \\ \frac{i}{Z_T} & 0 \end{pmatrix} \cdot \begin{pmatrix} 1 & 0 \\ \frac{i}{Z_S} & 1 \end{pmatrix} = \begin{pmatrix} -\frac{Z_T}{Z_S} & iZ_T \\ i \left(\frac{1}{Z_T} - \frac{Z_T}{Z_S^2} \right) & -\frac{Z_T}{Z_S} \end{pmatrix}$$

Any odd-window hybrid can be made by sandwiching the 1-window hybrid between sets of two transmission lines and a shunt on each side. Defining the zero-window hybrid to be a single shunt, we see that all even transmission lines can be found in a similar way. (Probably add a figure).

$$\mathbf{ABCD}_{e, n=0} = \begin{pmatrix} 1 & 0 \\ \frac{i}{z_s} & 1 \end{pmatrix}$$

Note that the ABCD matrices for both of these hybrids have purely imaginary off diagonal elements and identical, purely real on-diagonal elements. By induction, we see that all n-window hybrids share these properties:

$$\begin{aligned} \mathbf{ABCD}_{e, n} &= \begin{pmatrix} 1 & 0 \\ \frac{i}{z_s} & 1 \end{pmatrix} \cdot \begin{pmatrix} 0 & i z_T \\ \frac{i}{z_T} & 0 \end{pmatrix} \cdot \mathbf{ABCD}_{e, n-2} \cdot \begin{pmatrix} 0 & i z_T \\ \frac{i}{z_T} & 0 \end{pmatrix} \cdot \begin{pmatrix} 1 & 0 \\ \frac{i}{z_s} & 1 \end{pmatrix} \\ &= \begin{pmatrix} 1 & 0 \\ \frac{i}{z_s} & 1 \end{pmatrix} \cdot \begin{pmatrix} 0 & i z_T \\ \frac{i}{z_T} & 0 \end{pmatrix} \cdot \begin{pmatrix} a & i b \\ i c & a \end{pmatrix} \cdot \begin{pmatrix} 0 & i z_T \\ \frac{i}{z_T} & 0 \end{pmatrix} \cdot \begin{pmatrix} 1 & 0 \\ \frac{i}{z_s} & 1 \end{pmatrix} \\ &= \begin{pmatrix} -a + \frac{c z_T^2}{z_s} & -i c z_T^2 \\ -i \left(\frac{2a}{z_s} + \frac{b}{z_s^2} - \frac{c z_T^2}{z_s^2} \right) & -a + \frac{c z_T^2}{z_s} \end{pmatrix} = \begin{pmatrix} a' & i b' \\ i c' & a' \end{pmatrix} \end{aligned}$$

Rewriting the condition from before,

$$\begin{pmatrix} a_o & i b_o \\ i c_o & a_o \end{pmatrix} = \begin{pmatrix} \pm a_e & \mp i b_e \\ \mp i c_e & \pm a_e \end{pmatrix}$$

From Table 4.2,

$$\Gamma = \frac{\mathbf{A} + \mathbf{B} - \mathbf{C} - \mathbf{D}}{\mathbf{A} + \mathbf{B} + \mathbf{C} + \mathbf{D}}$$

$$\mathbf{T} = \frac{2}{\mathbf{A} + \mathbf{B} + \mathbf{C} + \mathbf{D}}$$

where A,B,C,D are the matrix elements. But since A=D, the conditions on Γ for even and odd:

$$\begin{aligned} \Gamma_e &= \mathbf{A}_e + \mathbf{B}_e - \mathbf{C}_e - \mathbf{D}_e = a_e + i b_e - i c_e - a_e = i (b_e - c_e) = 0 \\ \Gamma_o &= \mathbf{A}_o + \mathbf{B}_o - \mathbf{C}_o - \mathbf{D}_o = a_o + i b_o - i c_o - a_o = i (b_o - c_o) = \mp i (b_e - c_e) = 0 \end{aligned}$$

both yield the same information, that $b_o = c_o = \mp b_e = \mp c_e$. From the other condition,

$$|\mathbf{T}_e + \mathbf{T}_o| = |\mathbf{T}_e - \mathbf{T}_o|,$$

one finds

$$\begin{aligned} \left| \frac{2}{\mathbf{A}_e + \mathbf{B}_e + \mathbf{C}_e + \mathbf{D}_e} + \frac{2}{\mathbf{A}_o + \mathbf{B}_o + \mathbf{C}_o + \mathbf{D}_o} \right| &= \left| \frac{2}{\mathbf{A}_e + \mathbf{B}_e + \mathbf{C}_e + \mathbf{D}_e} - \frac{2}{\mathbf{A}_o + \mathbf{B}_o + \mathbf{C}_o + \mathbf{D}_o} \right|, \\ \left| \frac{1}{a_e + i b_e} + \frac{1}{a_o + i b_o} \right| &= \left| \frac{1}{a_e + i b_e} - \frac{1}{a_o + i b_o} \right|, \\ \left| \frac{1}{a_e + i b_e} \pm \frac{1}{a_e - i b_e} \right| &= \left| \frac{1}{a_e + i b_e} \mp \frac{1}{a_e - i b_e} \right|, \\ \left| \frac{2 a_e}{a_e^2 + b_e^2} \right| &= \left| \frac{2 b_e}{a_e^2 + b_e^2} \right|, \\ |a_e| &= |b_e| \end{aligned}$$

where we have used that $b_e = c_e$ and that $a_e = \pm a_o$, $b_e = \mp b_o$. We have thus found simple relations between all elements of either the even or odd ABCD matrix, which we will summarize below:

$$\begin{aligned} \mathbf{ABCD} &= \begin{pmatrix} \mathbf{A} & \mathbf{B} \\ \mathbf{C} & \mathbf{D} \end{pmatrix} = \begin{pmatrix} \mathbf{a} & \mathbf{i}\mathbf{b} \\ \mathbf{i}\mathbf{c} & \mathbf{a} \end{pmatrix} \\ \mathbf{b} &= \mathbf{c} \\ |\mathbf{a}| &= |\mathbf{b}| \end{aligned}$$

where a, b, c are all real. Note that there are only two constraint equations. Since an n -window hybrid has $n+1$ impedances, we expect there to be $n-1$ free impedances.

1-window Branchline Hybrid

We have already found the ABCD matrix for the 1-window hybrid:

$$\mathbf{ABCD}_e = \begin{pmatrix} -\frac{Z_T}{Z_S} & \mathbf{i}Z_T \\ \mathbf{i}\left(\frac{1}{Z_T} - \frac{Z_T}{Z_S^2}\right) & -\frac{Z_T}{Z_S} \end{pmatrix}$$

Using the relations from above:

$$\begin{aligned} \left| -\frac{Z_T}{Z_S} \right| &= |Z_T|, \quad \Rightarrow Z_S = 1 \\ \frac{1}{Z_T} - \frac{Z_T}{Z_S^2} &= Z_T \quad \Rightarrow Z_T = \sqrt{\frac{1}{1 + Z_S^2}} = \sqrt{\frac{1}{2}} \end{aligned}$$

Which is in agreement with the values given by Pozar.

2-window Branchline Hybrid

The ABCD matrix for the 2-window hybrid is:

$$\begin{aligned} \mathbf{ABCD}_e &= \begin{pmatrix} 1 & 0 \\ \frac{\mathbf{i}}{Z_{S2}} & 1 \end{pmatrix} \cdot \begin{pmatrix} 0 & \mathbf{i}Z_T \\ \frac{\mathbf{i}}{Z_T} & 0 \end{pmatrix} \cdot \begin{pmatrix} 1 & 0 \\ \frac{\mathbf{i}}{Z_{S1}} & 1 \end{pmatrix} \cdot \begin{pmatrix} 0 & \mathbf{i}Z_T \\ \frac{\mathbf{i}}{Z_T} & 0 \end{pmatrix} \cdot \begin{pmatrix} 1 & 0 \\ \frac{\mathbf{i}}{Z_{S2}} & 1 \end{pmatrix} \\ &= \begin{pmatrix} -1 + \frac{Z_T^2}{Z_{S1} Z_{S2}} & -\frac{\mathbf{i}Z_T^2}{Z_{S1}} \\ -\frac{2\mathbf{i}}{Z_{S2}} + \frac{\mathbf{i}Z_T^2}{Z_{S1} Z_{S2}^2} & -1 + \frac{Z_T^2}{Z_{S1} Z_{S2}} \end{pmatrix} \end{aligned}$$

Using the relations from above:

$$\begin{aligned} -\frac{2}{Z_{S2}} + \frac{Z_T^2}{Z_{S1} Z_{S2}^2} &= -\frac{Z_T^2}{Z_{S1}} \\ -2 Z_{S1} Z_{S2} + (1 + Z_{S2}^2) Z_T^2 &= 0 \\ Z_T^2 &= \frac{2 Z_{S1} Z_{S2}}{1 + Z_{S2}^2} \end{aligned}$$

which we can use to find

$$\begin{aligned} \left| -1 + \frac{Z_T^2}{Z_{S1} Z_{S2}} \right| &= \frac{Z_T^2}{Z_{S1}}, \\ \left| -1 + \frac{2}{1 + Z_{S2}^2} \right| &= \frac{2 Z_{S2}}{1 + Z_{S2}^2}, \\ |1 - Z_{S2}^2| &= 2 Z_{S2} \\ 0 &= \pm Z_{S2}^2 + 2 Z_{S2} \mp 1 \\ Z_{S2} &= \sqrt{2} \pm 1 \end{aligned}$$

and finally,

$$Z_T^2 = \frac{2 Z_{S1} (\sqrt{2} \pm 1)}{4 \pm 2\sqrt{2}} = \frac{Z_{S1}}{\sqrt{2}}$$

This is in agreement with the values found at www.microwaves101.com, except that they lack the $\sqrt{2} - 1$ solution. This solution tends to limit the bandwidth, and the goal of multiple windows is generally to enhance it, so one would understand why this solution would be neglected.

3-window Branchline Hybrid

The ABCD matrix for the 3-window hybrid is:

$$\begin{aligned} \mathbf{ABCD}_e &= \begin{pmatrix} 1 & 0 \\ \frac{i}{Z_{S2}} & 1 \end{pmatrix} \cdot \begin{pmatrix} 0 & i Z_{T2} \\ \frac{i}{Z_{T2}} & 0 \end{pmatrix} \cdot \begin{pmatrix} -\frac{Z_T}{Z_S} & i Z_T \\ i \left(\frac{1}{Z_T} - \frac{Z_T}{Z_S^2} \right) & -\frac{Z_T}{Z_S} \end{pmatrix} \cdot \begin{pmatrix} 0 & i Z_{T2} \\ \frac{i}{Z_{T2}} & 0 \end{pmatrix} \cdot \begin{pmatrix} 1 & 0 \\ \frac{i}{Z_{S2}} & 1 \end{pmatrix} \\ &= \begin{pmatrix} \frac{Z_T}{Z_S} + \frac{(Z_S^2 - Z_T^2) Z_{T2}^2}{Z_S^2 Z_{S2} Z_T} & -\left(\frac{i}{Z_T} - \frac{i Z_T}{Z_S^2} \right) Z_{T2}^2 \\ \frac{2 i Z_T}{Z_S Z_{S2}} - \frac{i Z_T}{Z_{T2}^2} + \frac{i Z_{T2}^2}{Z_S^2 Z_T} - \frac{i Z_T Z_{T2}^2}{Z_S^2 Z_{S2}^2} & \frac{Z_T}{Z_S} + \frac{Z_{T2}^2}{Z_{S2} Z_T} - \frac{Z_T Z_{T2}^2}{Z_S^2 Z_{S2}} \end{pmatrix} \end{aligned}$$

Using the relations from above:

$$\begin{aligned} \frac{2 Z_T}{Z_S Z_{S2}} - \frac{Z_T}{Z_{T2}^2} + \frac{Z_{T2}^2}{Z_{S2}^2 Z_T} - \frac{Z_T Z_{T2}^2}{Z_S^2 Z_{S2}^2} &= -\left(\frac{1}{Z_T} - \frac{Z_T}{Z_S^2} \right) Z_{T2}^2 \\ \Rightarrow Z_T^2 &= \frac{Z_S^2 Z_{T2}^4 + Z_S^2 Z_{S2}^2 Z_{T2}^4}{Z_S^2 Z_{S2}^2 - 2 Z_S Z_{S2} Z_{T2}^2 + Z_{T2}^4 + Z_{S2}^2 Z_{T2}^4} \end{aligned}$$

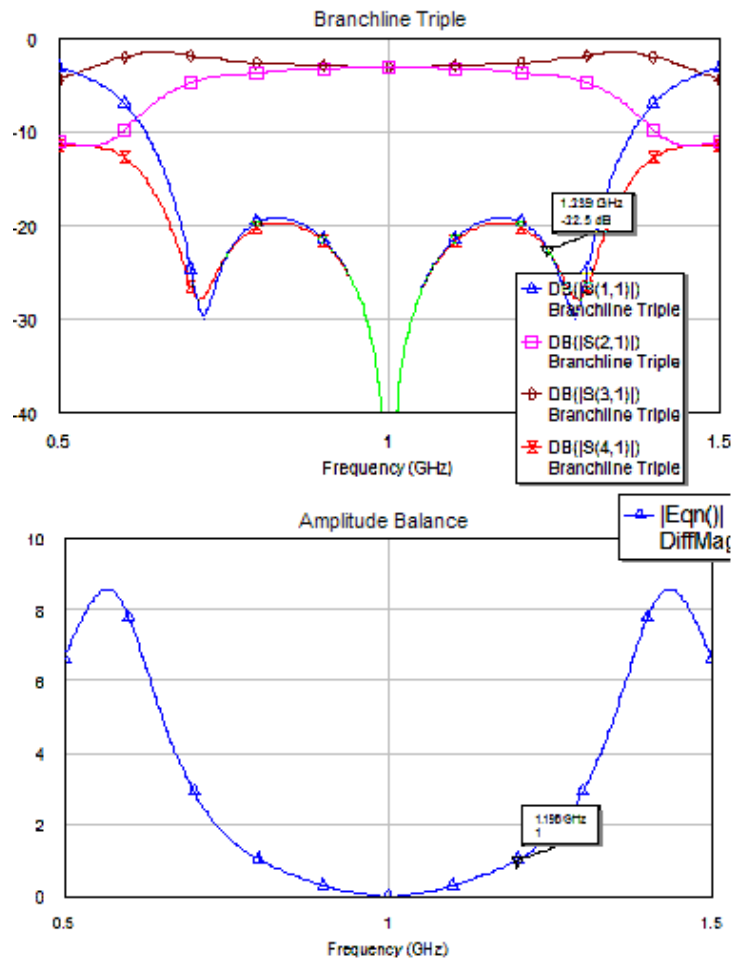
which we can use to find

$$\begin{aligned} \frac{Z_T}{Z_S} + \frac{Z_{T2}^2}{Z_{S2} Z_T} - \frac{Z_T Z_{T2}^2}{Z_S^2 Z_{S2}} &= -\frac{Z_{T2}^2}{Z_T} + \frac{Z_T Z_{T2}^2}{Z_S^2} \\ \Rightarrow Z_S &= \frac{2 Z_{T2}^2 \pm \frac{Z_{T2}^2}{Z_{S2}} \mp Z_{S2} Z_{T2}^2}{\pm 1 + Z_{S2}} = \frac{2 Z_{T2}^2 Z_{S2} \pm Z_{T2}^2 \mp Z_{S2}^2 Z_{T2}^2}{Z_{S2} (Z_{S2} \pm 1)} = Z_{T2}^2 \frac{2 Z_{S2} \pm 1 \mp Z_{S2}^2}{Z_{S2} (Z_{S2} \pm 1)} \\ &= Z_{T2}^2 \frac{(Z_{S2} \pm 1) + Z_{S2} (1 \mp Z_{S2})}{Z_{S2} (Z_{S2} \pm 1)} = Z_{T2}^2 \left(\frac{1}{Z_{S2}} \mp \frac{Z_{S2} \mp 1}{Z_{S2} \pm 1} \right) \end{aligned}$$

and finally,

$$Z_T = \frac{(-1 \mp 2 Z_{S2} + Z_{S2}^2) Z_{T2}^2}{\sqrt{2} Z_{S2}^2}$$

Based on the graphs below, I am relatively certain of this solution, even though I haven't found any results with which to compare. This is a 40% BW plot for the triple, which is 10% better than a double. For this and all branchline designs, increased BW can be achieved by relaxing the requirement of 3dB coupling at the center frequency by shifting the formulas for Z_T and Z_S by small amounts.



- $Z_T = 24 \Omega$
- $Z_{T2} = 33 \Omega$
- $Z_S = 49 \Omega$
- $Z_{S2} = 163 \Omega$

4-window Branchline Hybrid

The ABCD matrix for the 4-window hybrid is:

$$\begin{aligned}
\mathbf{ABCD}_e &= \begin{pmatrix} 1 & 0 \\ \frac{i}{Z_{S3}} & 1 \end{pmatrix} \cdot \begin{pmatrix} 0 & i Z_{T2} \\ \frac{i}{Z_{T2}} & 0 \end{pmatrix} \cdot \begin{pmatrix} -1 + \frac{Z_{T1}^2}{Z_{S1} Z_{S2}} & -\frac{i Z_{T1}^2}{Z_{S1}} \\ -\frac{2i}{Z_{S2}} + \frac{i Z_{T1}^2}{Z_{S1} Z_{S2}^2} & -1 + \frac{Z_{T1}^2}{Z_{S1} Z_{S2}} \end{pmatrix} \cdot \begin{pmatrix} 0 & i Z_{T2} \\ \frac{i}{Z_{T2}} & 0 \end{pmatrix} \cdot \begin{pmatrix} 1 & 0 \\ \frac{i}{Z_{S3}} & 1 \end{pmatrix} \\
&= \begin{pmatrix} \frac{Z_{S1} Z_{S2} (Z_{S2} Z_{S3} - 2 Z_{T2}^2) + Z_{T1}^2 (-Z_{S2} Z_{S3} + Z_{T2}^2)}{Z_{S1} Z_{S2}^2 Z_{S3}} & \frac{i (2 Z_{S1} Z_{S2} - Z_{T1}^2) Z_{T2}^2}{Z_{S1} Z_{S2}^2} \\ \frac{i (Z_{S2} Z_{S3} - Z_{T2}^2) (-Z_{T1}^2 Z_{T2}^2 + Z_{S2} (Z_{S3} Z_{T1}^2 + 2 Z_{S1} Z_{T2}^2))}{Z_{S1} Z_{S2}^2 Z_{S3}^2 Z_{T2}^2} & \frac{Z_{S1} Z_{S2} (Z_{S2} Z_{S3} - 2 Z_{T2}^2) + Z_{T1}^2 (-Z_{S2} Z_{S3} + Z_{T2}^2)}{Z_{S1} Z_{S2}^2 Z_{S3}} \end{pmatrix}
\end{aligned}$$

Using *Mathematica's* to solve for Z_{T1} , Z_{S2} and the conditions that

$$\begin{aligned}
\mathbf{b} &= \mathbf{c} \\
|\mathbf{a}| &= |\mathbf{b}|
\end{aligned}$$

one finds that

$$\begin{aligned}
Z_{S2} &= \frac{-1 + Z_{S3} (\pm 3 + \sqrt{2} | -1 \pm 2 Z_{S3} + Z_{S3}^2 |) - Z_{S3}^2 \mp Z_{S3}^3}{-1 \pm 2 Z_{S3} + Z_{S3}^2} \frac{Z_{T2}^2}{Z_{S3}} = \\
&= (1 + (\mp 1 + \sqrt{2} \text{Sign}[-1 \pm 2 Z_{S3} + Z_{S3}^2]) Z_{S3}) \frac{Z_{T2}^2}{Z_{S3}} \\
Z_{T1} &= \frac{\sqrt{Z_{S1} | -1 \pm 2 Z_{S3} + Z_{S3}^2 |}}{2^{1/4}} \frac{Z_{T2}}{Z_{S3}}
\end{aligned}$$

Unfortunately, the top solution limits bandwidth compared to the 3-window hybrid, and to enhance bandwidth with the bottom solution requires impedences we are not capable of creating ($\sim \frac{1}{2}$ to $\sim 9 Z_o$). We expect, then, that the 3-window solutions are then the best for practical purposes.

Appendix B

Code

The R code for the cubic splines is below. It takes data from a file: “w25 from 2.csv” which I made by saving the Excel file of the same name as a csv and fits S parameters as a function of the frequency in GHz. I used R because it is freely available and has an implementation of cubic splines already built into a library.

```

setwd("U:/ Jared/")
data <-read.table("w25 from 2.csv",sep=",",header=T)
names(data)

splineDesign(knots = 1:10, x=4:7)

s12.spline = lm(s12 ~ bs(data$GHz,knots = 1/2*(4:18)), data=data)
plot(x=data$GHz,y=data$s12,type="l")
s12.pred = predict(s12.spline,data.frame(data$GHz))
lines(data$GHz,s12.pred)

s22.spline = lm(s22 ~ bs(data$GHz,knots = 1/2*(4:18)), data=data)
plot(x=data$GHz,y=data$s22,type="l")
s22.pred = predict(s22.spline,data.frame(data$GHz))
lines(data$GHz,s22.pred)

s32.spline = lm(s32 ~ bs(data$GHz,knots = 1/2*(4:18)), data=data)
plot(x=data$GHz,y=data$s32,type="l")
s32.pred = predict(s32.spline,data.frame(data$GHz))
lines(data$GHz,s32.pred)

s42.spline = lm(s42 ~ bs(data$GHz,knots = 1/2*(4:18)), data=data)
plot(x=data$GHz,y=data$s42,type="l")
s42.pred = predict(s42.spline,data.frame(data$GHz))
lines(data$GHz,s42.pred)

launcher.spline = lm(S12_day2_10db ~ bs(data$GHz,knots = 1/2*(4:18)), data=data)
plot(x=data$GHz,y=data$S12_day2_10db,type="l")
launcher.pred = predict(launcher.spline,data.frame(data$GHz))
lines(data$GHz,launcher.pred)

plot(x=1:10,y=(0:9)*(-5),type="n")
lines(data$GHz,s12.pred)
lines(data$GHz,s22.pred)
lines(data$GHz,s32.pred)
lines(data$GHz,s42.pred)

stuff = cbind(s12.pred,s22.pred,s32.pred,s42.pred,launcher.pred)
write.csv(stuff,"fitted.csv")

```

After putting the data into a format that lists the data as: Frequency, S11, S12, S13, S14, S21, S22, etc, I used the following Excel macro to put it into a format that MWO prefers,

a Touchstone 4 port (.s4p). This would be better done in a scripting language, but I know none.

```
Sub From_mdf_to_Touchstone()  
  For j = 0 To 1600  
    i = 6 + 4 * j  
    Rows(i & ":" & i).Select  
    Selection.Insert Shift:=xlDown  
    Selection.Insert Shift:=xlDown  
    Selection.Insert Shift:=xlDown  
    Range("J" & i - 1 & ":Q" & i - 1).Select  
    Selection.Cut  
    Range("B" & i).Select  
    ActiveSheet.Paste  
    Range("R" & i - 1 & ":Y" & i - 1).Select  
    Selection.Cut  
    Range("B" & i + 1).Select  
    ActiveSheet.Paste  
    Range("Z" & i - 1 & ":AG" & i - 1).Select  
    Selection.Cut  
    Range("B" & i + 2).Select  
    ActiveSheet.Paste  
  Next j  
End Sub
```